Pergamon

NanoStructured Materials, Vol. 4, No. 2, pp. 169-182, 1994

0965-9773/94 $6.00 + .00

PROCESSING OF NANOCOMPOSITE SILICON NITRIDE-MULLITE-ALUMINA BY REACTION SINTERING

Y. Sakka* and **I.A. Aksay****

*Chemical Processing Division, National Research Institute for Metals
2-1, Sengen-1, Tsukuba, Ibaraki 305, Japan
**Department of Chemical Engineering and Princeton Materials Institute
Princeton University, Princeton, NJ 08544-5263

(Accepted February 1994)

Abstract—*We describe a new method for processing Si_3N_4-mullite-Al_2O_3 nanocomposites by reaction sintering of the green compacts after partial oxidation treatment. Bimodal powder compacts used in this process were prepared by a colloidal filtration method. Si_3N_4 and Al_2O_3 powders were dispersed in aqueous suspensions at pH=10 with the aid of an electrosteric stabilizer, polymethacrylic acid. A binary mixture of Al_2O_3 powder was used to attain high green densities. This process results in the following morphology: nanometer-sized Si_3N_4 particles that are distributed in the mullite phase which is embedded in an Al_2O_3 matrix.*

I. INTRODUCTION

Advanced ceramic matrix composites are used in many fields, such as electronic, structural, or biomaterial applications. Recently, ceramic matrix nanocomposites have been receiving increasing attention largely due to their significantly enhanced mechanical properties, low-temperature densification, machinability, and superplastic behavior (1-3). Nanocomposites can be classified into two general categories (3). One category consists of composites of only nanometer-sized grains. The other consists of composites where nanosized particles are distributed within the intra-and/or intergrain regions of micron-sized grains. The main advantage of using nanocomposites of the first category is that they can be shaped by superplastic deformation, whereas the main advantage of the nanocomposites of the second category is their enhanced high temperature stability against grain coarsening and mechanical properties. In this paper, we deal with the processing of the second type of nanocomposite with a novel reaction sintering method.

In a recent study, we illustrated the use of reaction sintering as an economical and reliable method for the processing of SiC-mullite-Al_2O_3 nanocomposites (4,5). In this study, we extend this technique to the processing of Si_3N_4-mullite-Al_2O_3 nanocomposites. Our procedure consists of three steps shown in Figure 1 (4,5). First, we consolidate submicron-sized Si_3N_4 and Al_2O_3 powders homogeneously through colloidal consolidation. For the composite material processing of submicron size powder, colloidal dispersion and consolidation techniques have high potential

in controlling pore volume and pore size distribution of compacts and achieving a desired microstructure (6,7).

Here, the effect of using bimodal Al_2O_3 powders (8-10) on the microstructure of the green compacts is also examined. Second, partial oxidation treatment is conducted to oxidize the surface of the Si_3N_4 particles to SiO_2. This reduces the size of the Si_3N_4 particles to nanometer size. Finally, we react the surface oxide and Al_2O_3 to produce mullite. As we illustrate in the following sections, the advantages of this method are that (1) the reduction of the inclusion phase to nanoscale can be achieved without milling, (2) due to a volume increase during reaction sintering, the sintering shrinkage is low, and (3) since the oxidation product silica is in amorphous form, the viscous deformation of silica allows the densification process to occur at lower temperatures (11,12), and aids in the formation of dense sintered bodies without pressure.

II. EXPERIMENTAL PROCEDURE

Two types of α-Al_2O_3 powders were used in this study, Sumitomo Chemical's high-purity alumina ($\geq$ 99.995%): the fine powder (AKP-50, indicated as Al_2O_3(F)) with a mean particle diameter of 0.21 μm and specific surface area of 9.5 m^2/g, and the coarse powder (AKP-15, indicated as Al_2O_3(C)) with a mean particle diameter of 0.78 μm and specific surface area of 2.4 m^2/g. Bimodal powder where the ratio of Al_2O_3(C) to Al_2O_3(F) was 7/3 is designated as Al_2O_3(B). The Si_3N_4 powder used was Ube Industries' α-Si_3N_4 (SN-E10; α content above 95%) with a mean particle diameter of 0.2 μm and specific surface area of 10.0 m^2/g. The data presented here for the alumina and silicon nitride are the manufacturer's reported data except the specific surface area. The specific surface areas were measured by standard BET N_2 adsorptions.

Stable colloidal suspensions with a solids content of 45 vol% were prepared electrosterically in distilled water with an NH_4 salt of polymethacrylic acid (PMAA, Darvan C) at pH = 10 as described in the next section. NH_4OH was used to adjust the pH. After ultrasonic vibration (Sonic Materials Vibracell 600W Unit, Danbury, CT) was applied for 10 min to facilitate the dispersion of the powders agglomerates, the suspension was stirred for over 12 h at room temperature. Degassing of the suspension was performed in a bell jar connected to a vacuum pump for about 30 min. A colloidal consolidation technique (slip cast) employing a gypsum mold was used to consolidate the colloidal particles. The compacts were then dried overnight at 100°C.

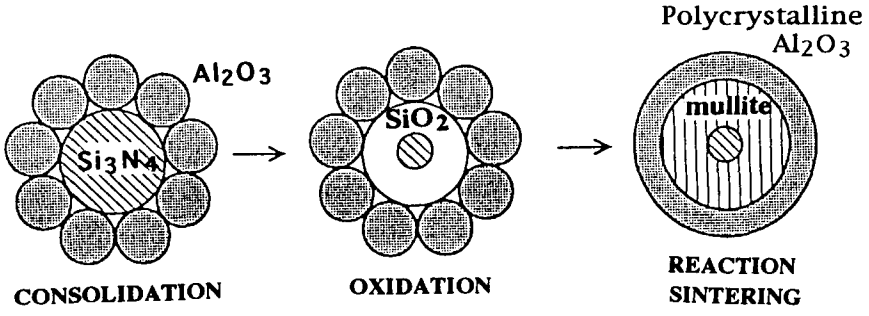

Figure 1. Schematic illustration of the process steps used to produce nanocomposites by reaction sintering.

Rheological properties of the suspensions were measured by a cone and plate viscometer (Visconic EMD type, Tokyo Keiki Co., Tokyo, Japan) at 20°C as a function of shear rate over a range of shear rates of 1.92 to 383 s^{-1}.

Thermogravimetric analysis (TGA; TGA7 Thermogravimetric analyzer, Perkin Elmer, Norwalk, CT) was conducted to determine the oxidation level of the Si_3N_4 by weight increase. The dried compacts were put in a platinum pan and heated to soaking temperatures between 1000 and 1300°C at a heating rate of 10°C/min in a stream of dry air. Reaction between the Pt and the Si_3N_4 powder was not observed.

The reaction sintering for the samples after partial oxidation treatment in air was conducted in an alumina crucible in a stream of Ar (above 99.9 % purity) using a graphite furnace at a heating rate of 25°C/min and a cooling rate of 5°C/min. The densities of the green compacts and the sintered bodies were measured by the Archimedes' method using kerosene or distilled water, respectively. Pore channel size distribution of the compacts was investigated by mercury porosimetry (9,10). The pore channel size distribution was obtained using standard values for the mercury surface energy (0.48 N/m) and the contact angle (140°). Phase analysis was conducted by X-ray diffraction (XRD; X-ray Diffractometer, Rigaku RU-300, Tokyo, Japan) using Ni-filtered CuKα radiation.

Sintered samples were polished down to 1 μm surface finish with diamond paste and then thermally etched at 1450°C for 20 min in an Ar atmosphere. The resulting microstructures were evaluated by scanning electron microscopy (SEM; Philips 515 Scanning Electron Microscope) and transmission electron microscopy (TEM; Philips 300 Transmission Electron Microscope). A coating of gold and palladium was sputtered on the surface of the samples for SEM.

III. RESULTS AND DISCUSSION

Dispersion and Consolidation

In the preparation of the colloidal suspensions, controlling the interactions between particles has a significant influence on the stability of a suspension. In our system, an electrosteric stabilization approach was preferred over an electrostatic one since it was not possible to disperse both Si_3N_4 and Al_2O_3 equally well at the same pH level. When only electrostatic dispersion was used, Si_3N_4 dispersed best under basic conditions, whereas Al_2O_3 dispersed best under acidic conditions (13-16). Consequently, an NH_4 salt of PMAA was used as an electrosteric stabilizer (0.4 g/m^2) (13,14) to improve the stability of Al_2O_3 under basic conditions so that a low viscosity composite suspension could be prepared at pH = 10. Figure 2 shows the rheological behavior of the Al_2O_3(F)-15Si_3N_4 suspensions with and without the PMAA. A significant decrease in viscosity of the 45 vol% solids suspension with PMAA is seen in comparison with 30 vol% solids suspension without PMAA. Adding PMAA decreased the viscosity significantly, which indicates the suspension dispersion is significantly improved. Figure 3 shows the rheological behavior of 45 vol% solids suspensions using the three types of Al_2O_3 powders. All the suspensions were fluid enough for slip casting and the suspension with bimodal Al_2O_3 had the lowest viscosity due to space filling of smaller particles into a matrix of larger particles. At a fixed solids content, nearly an order of magnitude decrease in viscosity can be realized simply with addition of smaller particles into a nearly monosized matrix (29).

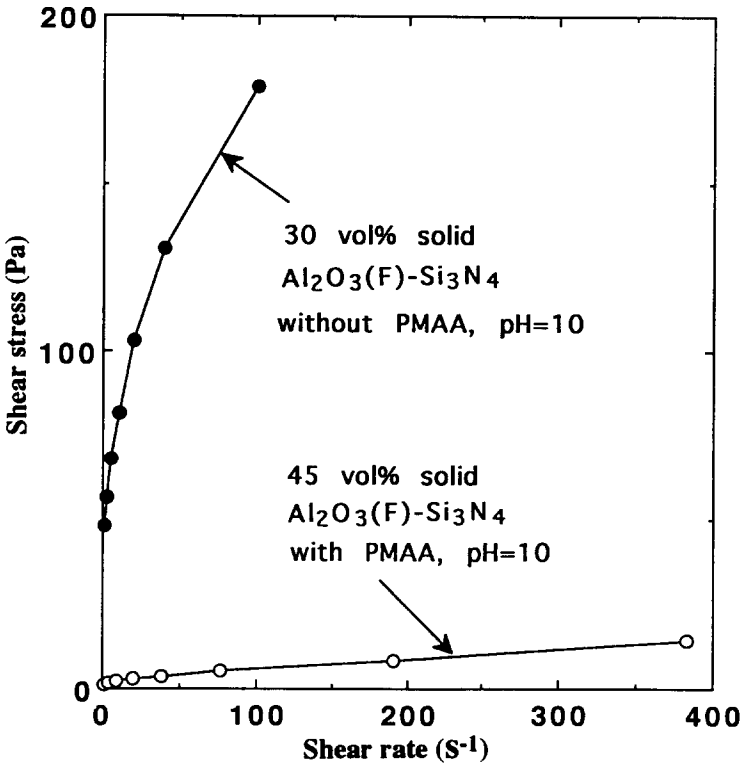

Figure 2. The shear stress-shear rate relation for the 45 vol% solids Al_2O_3(F)-15Si_3N_4 with PMAA and the 30 vol% solids Al_2O_3(F)-15Si_3N_4 without PMAA.

During colloidal consolidation of multi-component suspensions, a key problem is the segregation of particles either due to gravitational (9,10,17) or thermodynamic phase separation (18,19) effects. The best solution for minimizing particle segregation is to prepare the suspensions as highly concentrated as possible (9,10,17-19). Since significant segregation and/or phase separation did not occur while using a 45 vol% solid suspension of Al_2O_3-SiC systems (5), we also prepared 45 vol% solid suspensions in this system. Homogeneous microstructure (Figure 4) and narrow pore channel size distributions (Figure 5) were obtained with all these compacts. The relative green densities of Al_2O_3(F)-15Si_3N_4, Al_2O_3(B)-15Si_3N_4 and Al_2O_3(C)-15Si_3N_4 were 61.5, 65.7 and 65.1%, respectively. Increase of density in Al_2O_3(B)-15Si_3N_4 system is not significant in comparison with that in Al_2O_3(C)-15Si_3N_4 system. This may be due to the fact that the mixtures of Al_2O_3(C) and Si_3N_4 are a binary combination of the coarse Al_2O_3 and the fine Si_3N_4 powders and thus they also display the advantages of binary mixtures.

Oxidation Process

A typical weight loss during heating Al_2O_3(F)-15Si3N_4 at a heating rate of 10°C/min is shown in Figure 6. Upon heating to 700°C weight loss was observed in two regions; in the first

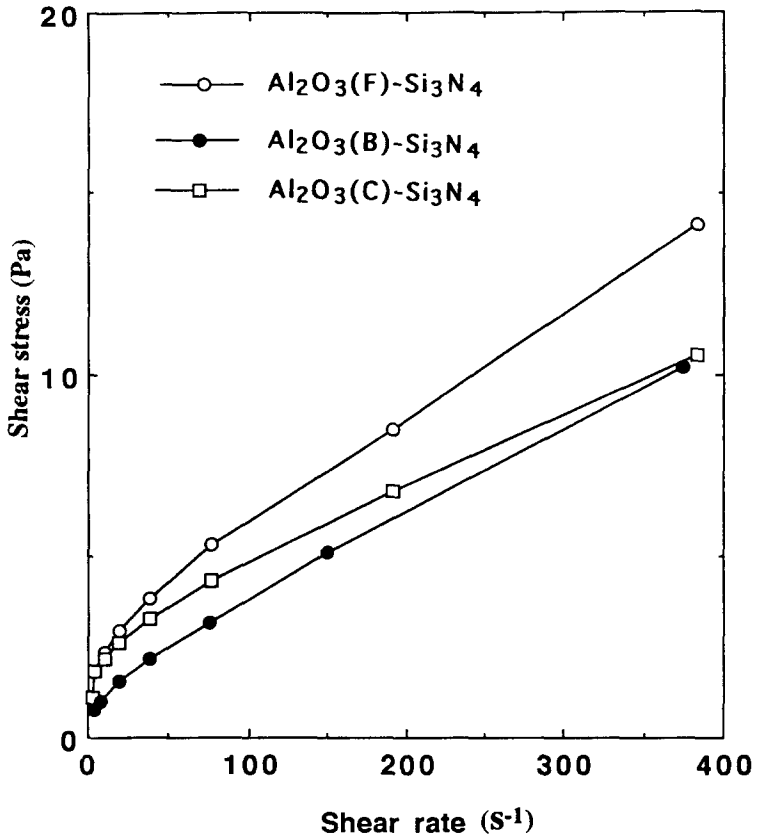

Figure 3. The shear stress-shear rate relation for the 45 vol% solids Al_2O_3-15Si_3N_4 systems.

region (up to 300°C) the weight decrease is due to the desorption of water and the second region (around 350°C) is mainly due to decomposition of the surfactant. Above 500°C, the weight loss reaches a maximum value, and due to the onset of Si_3N_4 oxidation, a weight gain is observed at higher temperatures. The plateau value at the maximum weight loss was used as the reference point to determine the fraction of silica that forms as the oxidation product on the surface of the Si_3N_4 particles.

The size of the Si_3N_4 core particles was controlled by determining the fraction of Si_3N_4 oxidized during heat treatment. Figure 7 shows the oxidation fraction in weight. The oxidation behavior of the Si_3N_4 powder in this temperature range is believed to follow a passive oxidation reaction (20):

$$Si_3N_4 + 3O_2 \rightarrow 3SiO_2 + 2N_2 \qquad [1]$$

Many authors have reported that oxidation of Si_3N_4 powders in various oxidizing atmospheres follows parabolic kinetics (21-24). The oxidation fraction is represented by the following Jander's equation (25).

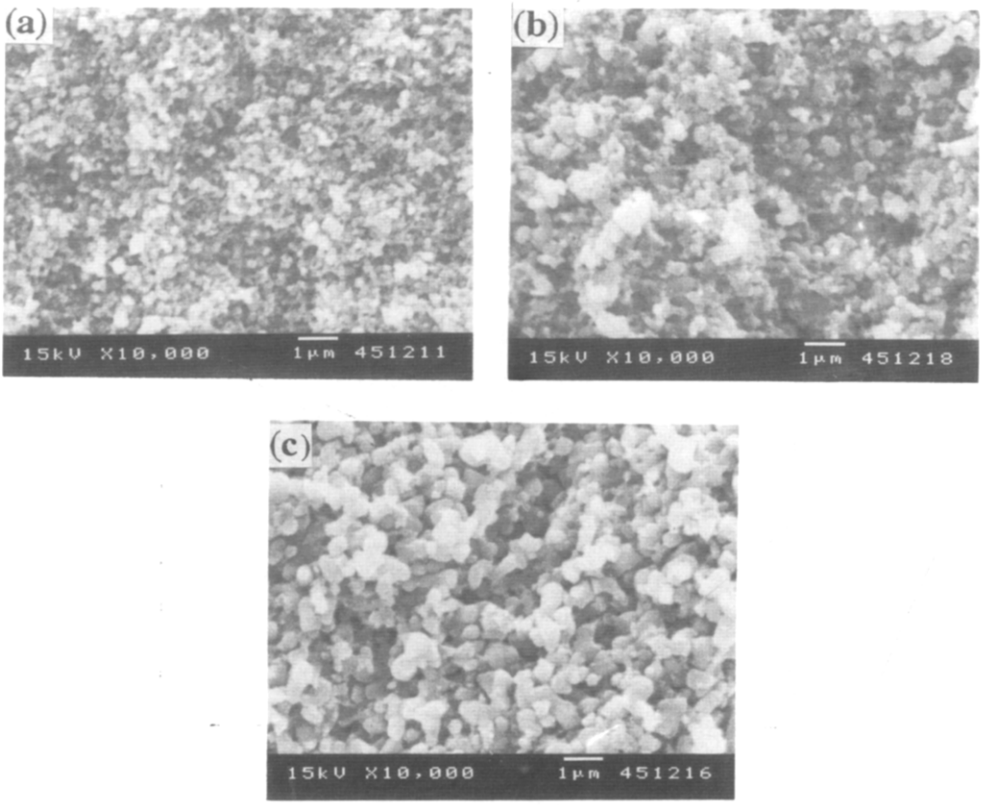

Figure 4. SEM images of the fractured surfaces of (a) Al_2O_3(F)15Si_3N_4, (b) Al_2O_3(B)-15Si_3N_4,and (c) Al_2O_3(C)-15Si_3N_4 after consolidation.

$$1 - (1- f)^{1/3} = (kt)^{1/2} \qquad [2]$$

where f is the oxidation fraction, t is the reaction time, and k is the rate constant. As shown in Figure 8, when the $[1 - f)^{1/3}]$ is plotted versus the square root of time, a linear variation is observed, suggesting that oxidation is rate limited by a diffusion process. Using eq. [2] we can calculate the rate constants at every temperature. An Arrhenius plot of the rate constants in the temperature range of 1000-1300°C is shown in Figure 9. The activation energy for Al_2O_3(F)-Si_3N_4 system is 340 kJ/mol. Activation energies reported in the literature vary from 250 to 480 kJ/mol (21-24). This large amount of scatter has been attributed to the different types of materials (powder, poly-crystal and single-crystal), with varying concentrations of impurities, which can alter the oxidation kinetics significantly. The activation energies obtained in our study are close to the activation energy of the oxygen diffusion in vitreous silica (298 kJ/mol) (26) but not to that of the molecular oxygen diffusion (113 kJ/mol)(27), or not to the formation of an intermediate phase Si_2N_2O (480 kJ/mol) (24). The present oxidation reaction seems to proceed via oxygen diffusion through the silica film.

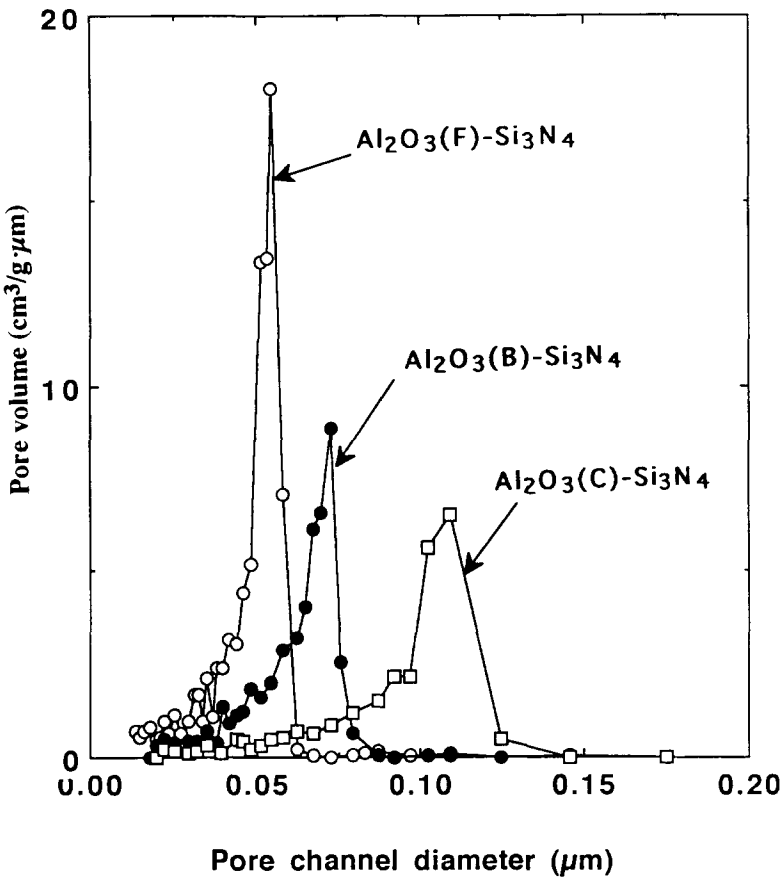

Figure 5. Hg porosimetry pore channel size distributions of the Al_2O_3-15Si_3N_4 compacts consolidated by the colloidal consolidation.

Figure 10 shows the X-ray diffraction patterns of Al_2O_3-15Si_3N_4 oxidized at 1300°C for 2 h in air. The decrease in the amount of Si_3N_4 can be seen from the figure, where amorphous SiO_2 might be produced as is the case of Al_2O_3-SiC system using fine powders (5).

Reaction Sintering and Microstructure

The comparison of the X-ray diffraction patterns in Figure 10 confirms the premise of this study, that SiO_2 phase is formed as the oxidation product and is then consumed to form mullite during the final stage heat treatment in Ar. Transformation of α-Si_3N_4 to β-Si_3N_4 was observed for the samples sintered at 1700°C but not at 1600°C. The existence of Si_2N_2O phase is not observed.

In calculating the theoretical densities of the compacts, two types of volume expansion had to be considered (28). Volume expansion of Si_3N_4 upon oxidation is 76% and formation of stoichiometric mullite from the reaction of $3Al_2O_3$ and $2SiO_2$ results in a volume increase of 5% (5). The theoretical densities were determined by the following equation:

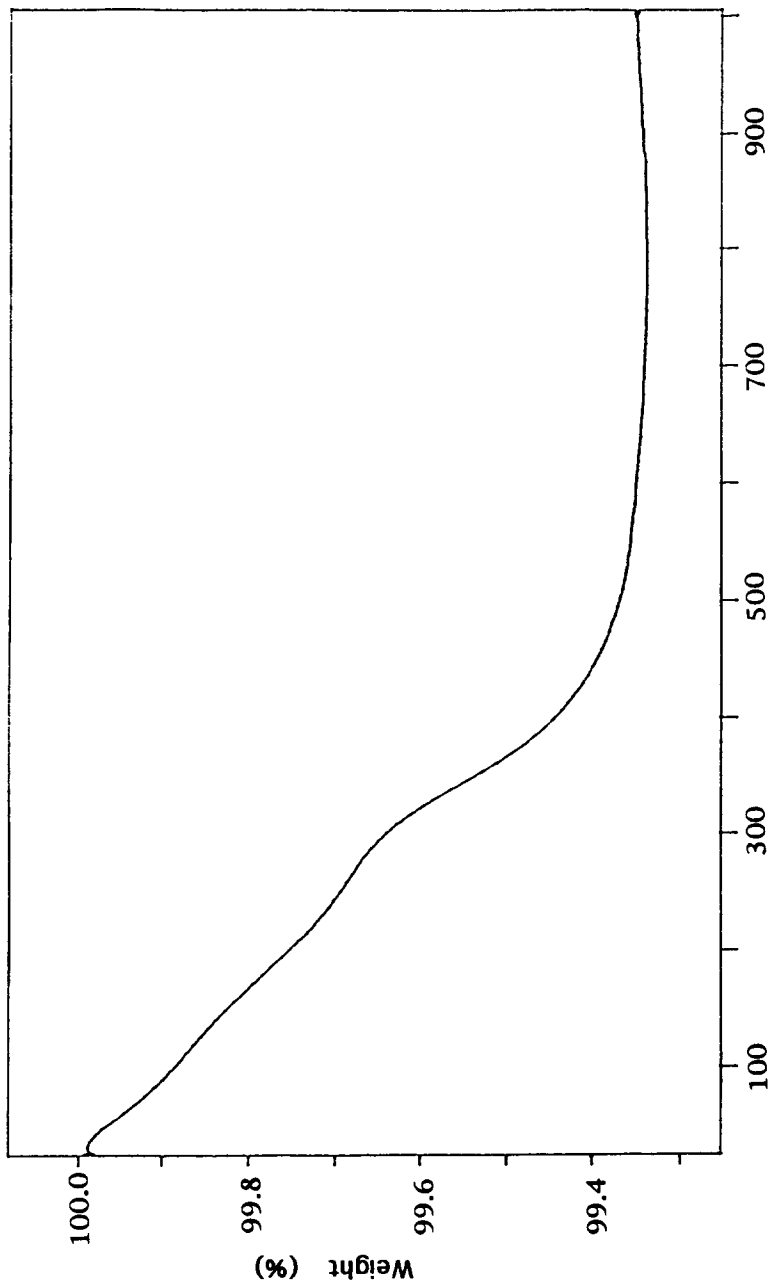

Figure 6. TGA curves of colloidal consolidated compacts of Al_2O_3(F)-15Si_3N_4 at a heating rate of 10°C /min in a stream of dry air.

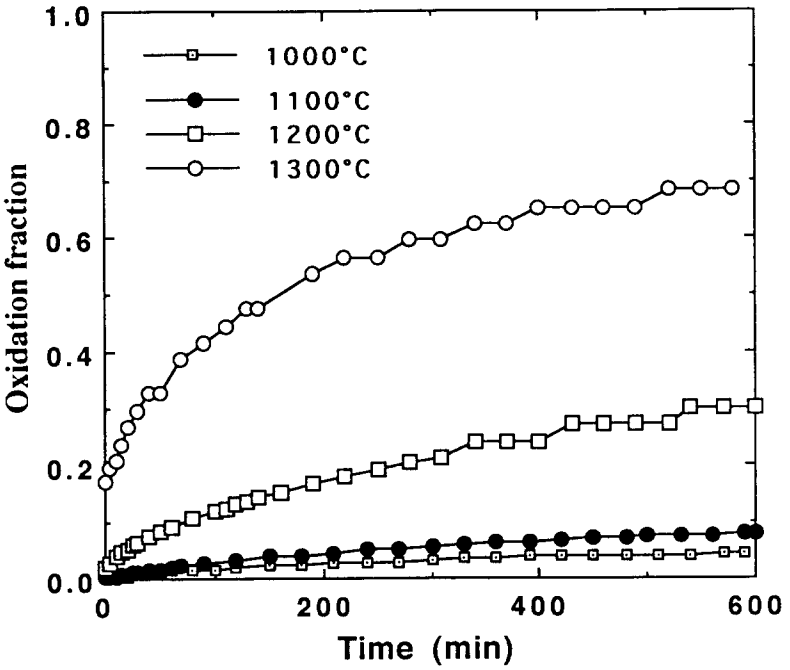

Figure 7. Oxidation fraction in weight of Al_2O_3(F)-15Si_3N_4 system during isothermal holding in a stream of dry air.

$$\rho = [V_s\rho_s + (1\text{-}V_s)\rho_A]W/K \quad [3]$$

where ρ_s and ρ_A are the theoretical densities of Si_3N_4 and Al_2O_3, respectively, V_s the volume fraction of Si_3N_4, and W is the oxidation weight increase ratio. K is a factor controlled by the composition and the respective volume expansions, as

$$K = \frac{fv_s(1.76 \times 1.05 - 1)}{[1 + (1-f)V_s]} + 1 \quad [4]$$

where f is the oxidation fraction of Si_3N_4. The linear shrinkage L is calculated by the following equation:

$$L = (K\,\rho_o/\,\rho)^{1/3} - 1 \quad [5]$$

where ρ_o is the green density. It is easily calculated using above equation that sinter shrinkage is lower due to the two types of volume increase.

Figure 11 shows the relative sintered densities of the samples which partially oxidized at 1300°C for 2 h and reaction-sintered at 1600°C for 2 h. Higher sintered densities were obtained by sintering at 1600°C for 2h in an Ar atmosphere without pressure. As is the case in transient

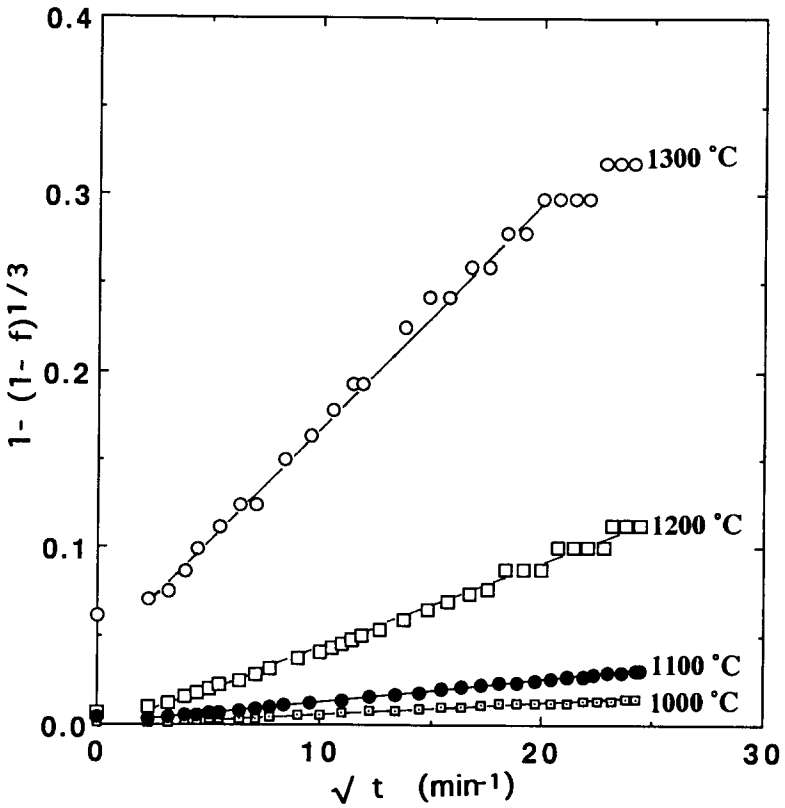

Figure 8. Relationship between square root of time and $[1-(1-f)^{1/3}]$ for Al_2O_3(F)-15Si_3N_4 composites during isothermal holding in a stream of dry air.

viscous phase processing of mullite in homogeneously mixed compacts of amorphous SiO_2 and Al_2O_3 powders (11,12), viscous deformation of silica is the most likely mechanism contributing to the enhanced densification of the compacts in this study.

Figure 12 shows a SEM image of a polished and etched Al_2O_3(F)-15Si_3N_4-mullite sample that was oxidized at 1300°C and sintered at 1600°C for 2h. At this resolution, although small second phase inclusions are observed, it is not obvious whether these inclusions extend to the nanoscale range. Figure 13 shows a TEM image of the same samples of Figure 12. Nanometer-sized spherical Si_3N_4 particles are observed as inclusions within a mullite matrix as confirmed by energy dispersive X-ray spectroscopy (EDS). This morphology shows that the surface of the Si_3N_4 is oxidized uniformly and nanometer-sized Si_3N_4 particles remain in the mullite matrix as illustrated in Figure 1.

IV. CONCLUSIONS

Si_3N_4-mullite-Al_2O_3 nanocomposites were processed through a novel colloidal consolidation and reaction sintering process. First, micron-sized Si_3N_4 and Al_2O_3 particles were colloidally

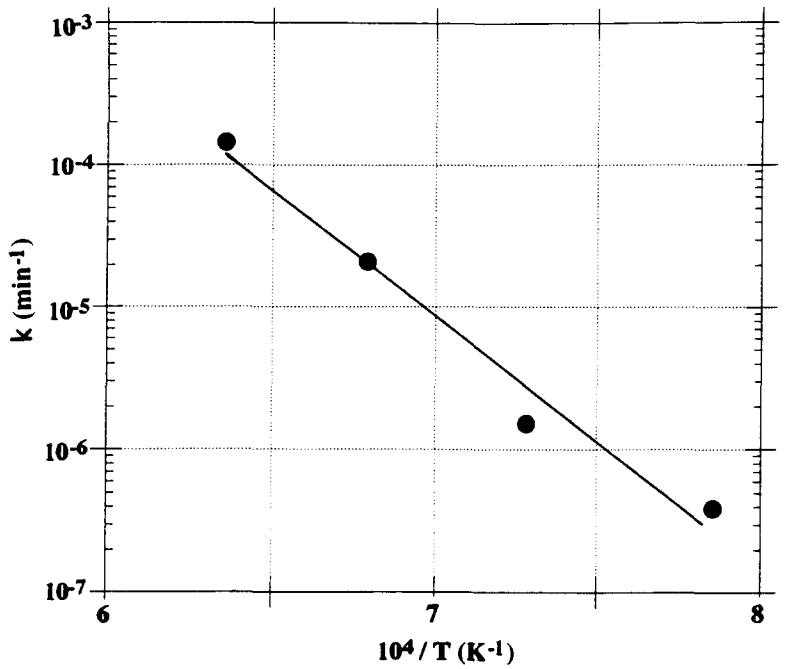

Figure 9. Arrhenius plot of the passive oxidation rate constants.

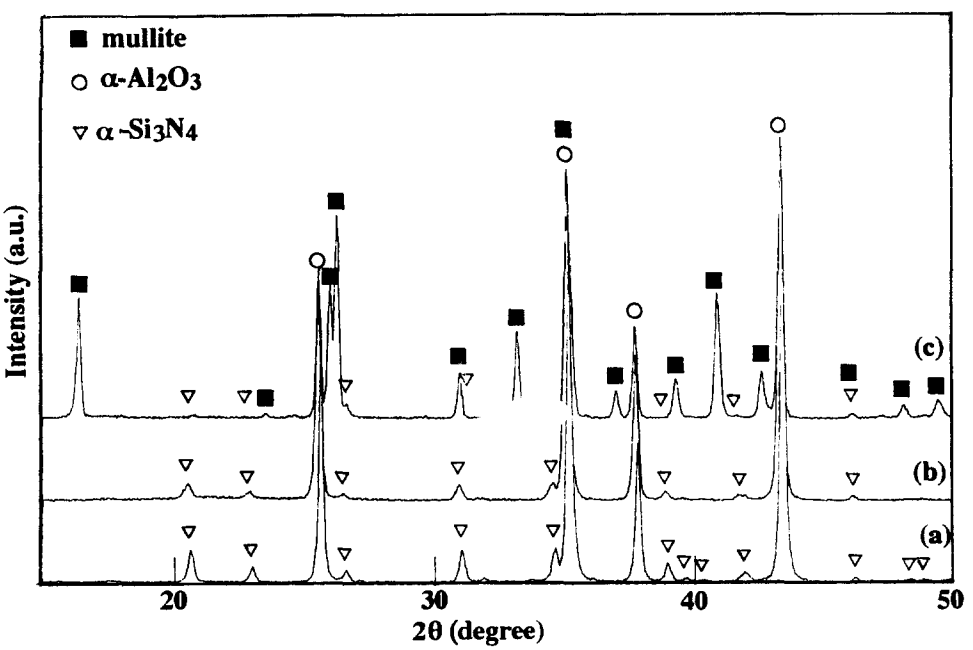

Figure 10. X-ray diffraction patterns of Al_2O_3(F)-15Si_3N_4 (a) as colloidal consolidation, (b) after oxidation, and (c) after reaction sintering at 1600°C for 2 h in Ar.

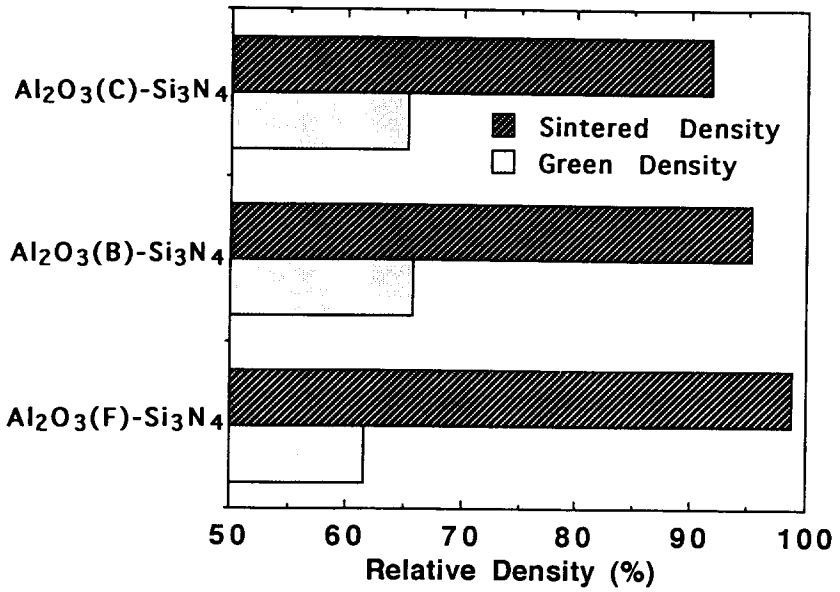

Figure 11. Density after an initial oxidation at 1300°C in air and then a final sintering at 1600°C for 2 h in Ar.

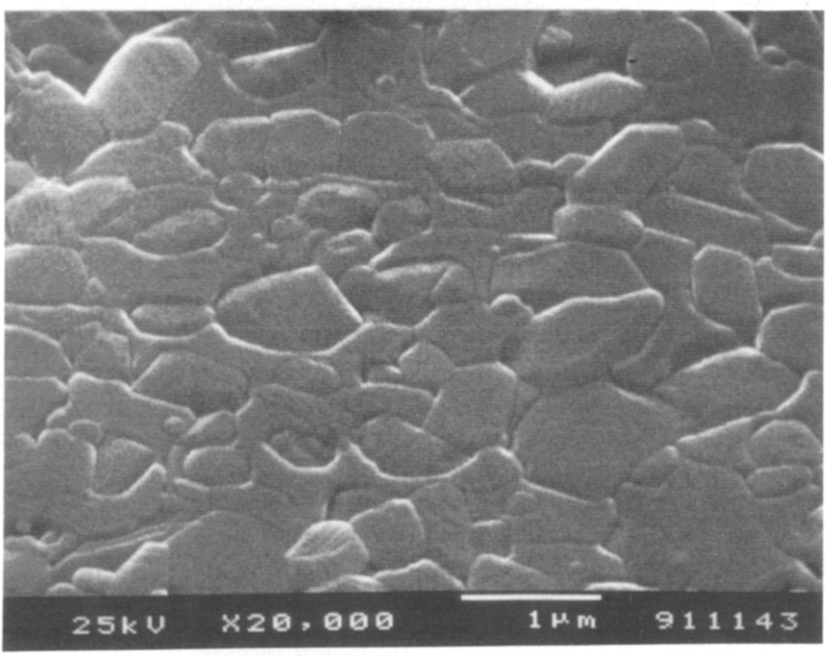

Figure 12. SEM image of polished and a thermally etched Al_2O_3(F)-15Si_3N_4-mullite nanocomposite first oxidized at 1300°C for 2 h and followed by a 1600°C sintering for 2 h in Ar.

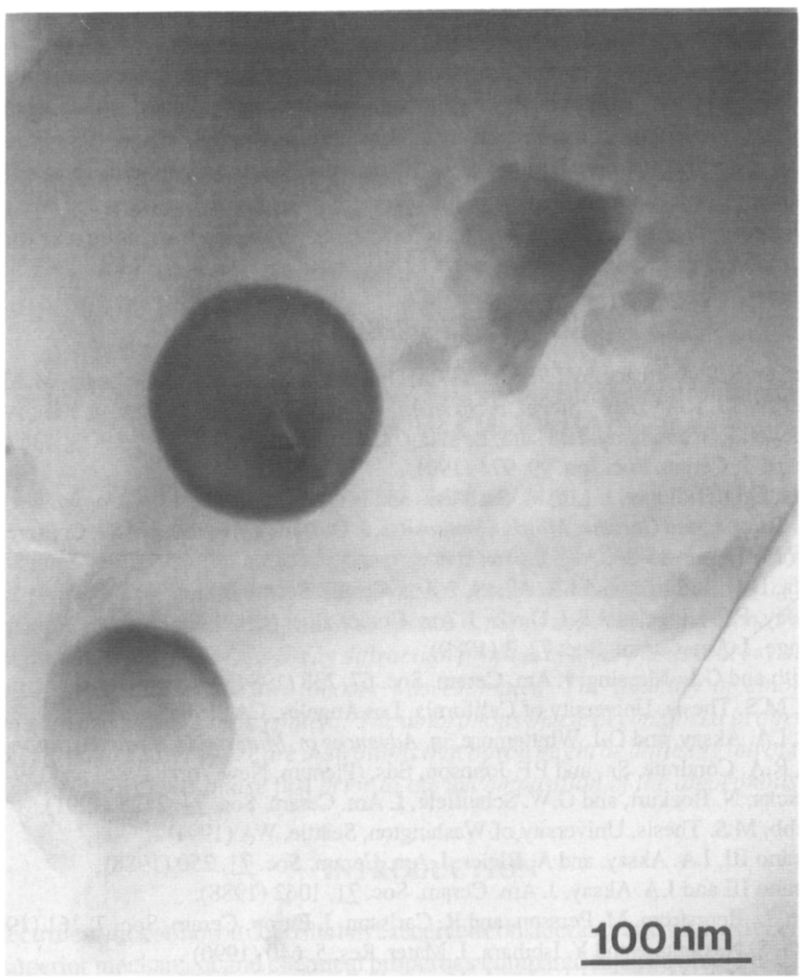

Figure 13. TEM image of Al_2O_3(F)-Si_3N_4-mullite nanocomposites first oxidized at 1300°C for 5 h in air and followed by final sintering treatment at 1600°C for 2h in Ar. (Spherical particles are Si_3N_4.)

dispersed and consolidated to form uniformly mixed compacts. Second, Si_3N_4 particles were partially oxidized until the Si_3N_4 particles was reduced to a nanometer-sized core. Third, these nanometer-sized core particles were trapped within a mullite matrix as the silica oxidation product reacted with the alumina to form the mullite matrix.

This process offers several advantages and thereby warrants further research: (1) it eliminates the need to reduce the particle size of the inclusion phase to the nanometer range by milling and thus provides better control in minimizing impurities; (2) due to volume increase during reaction sintering, sintering shrinkage are lower, and (3) the presence of amorphous silica as a transient phase results in enhanced densification by viscous deformation and thus provides an opportunity to process these composites without pressure.

ACKNOWLEDGEMENTS

This work was supported by the U.S. Air Force Office of Scientific Research under Grant No. AFOSR-F49620-93-1-0259. The main part of this work was conducted at the Department of Materials Science and Engineering, University of Washington, Seattle, WA 98195. We acknowledge M. Sarikaya and J. Liu of the University of Washington for their help with TEM observation and T. Takahashi of NRIM for his help with measuring the rheological properties. We also wish to thank D.D. Bidinger, L. Bergström, M. Yasrebi, C.H. Schilling and K. Shinozaki for the help in performing the experiment.

REFERENCES

1. R.P. Andres, R.S. Averback, W.L. Brown, W.A. Goddard III, A. Kaldor, S.G. Louie, M. Moscovits, P.S. Peercy, S.J. Riley, R.W. Siegel, F. Spaepen, and Y. Wang, J. Mater. Res. 4, 705 (1989).
2. R.W. Siegel, R. Ramasamy, H. Hahn, L. Tiang, and R. Gronsky, J. Mater. Res. 3, 1367 (1988).
3. K. Niihara, J. Ceram. Soc. Jpn. 99, 974 (1991).
4. Y. Sakka, D.D. Bidinger, J. Liu, M. Sarikaya, and I.A. Aksay, in *The 16th Conference of Metal Matrix, Carbon, and Ceramic Matrix Composites*, J. D. Buckley, editor, NASA Conference Publ. #3175, (1992) pp. 15-26.
5. Y. Sakka, D.D. Bidinger and I.A. Aksay, J. Am. Ceram. Soc., in press.
6. I.A. Aksay, F.F. Lange, and B.I. Davis, J. Am. Ceram. Soc. 60, C190 (1983).
7. F.F. Lange, J. Am. Ceram. Soc. 72, 3 (1989).
8. J.P. Smith and G.L. Messing, J. Am. Ceram. Soc. 67, 238 (1984).
9. C. Han, M.S. Thesis, University of California, Los Angeles, CA (1985).
10. C. Han, I.A. Aksay, and O.J. Whittemore, in *Advances in Materials Characterization II*, R.L. Snyder, R.A. Condrate, Sr., and P.F. Johnson, Eds. (Plenum, New York, 1985) pp. 339-47.
11. M.D. Sacks, N. Bozkurt, and G.W. Scheiffele, J. Am. Ceram. Soc. 74, 2428 (1991).
12. J.E. Webb, M.S. Thesis, University of Washington, Seattle, WA (1991) .
13. J. Cesarano III, I.A. Aksay, and A. Bleier, J. Am. Ceram. Soc. 71, 250 (1988).
14. J. Cesarano III and I.A. Aksay, J. Am. Ceram. Soc. 71, 1062 (1988).
15. E. Liden, L. Bergström, M. Persson, and R. Carlsson, J. Europ. Ceram. Soc. 7, 361 (1990).
16. Y. Hirata, S. Nakagame and Y. Ishihara, J. Mater. Res. 5, 640 (1990) .
17. Y. Hirata and I.A. Aksay, in *Advances in Materials, Processing and Manufacturlng, Proceedings of the Advanced Materials Technology Ceramic Workshop*, Number 4 (International Committee for Advanced Materials Technology, Nagoya, Japan, 1988) pp. 3-15.
18. J. Liu, W.Y. Shih, R. Kikuchi, and I.A. Aksay, J. Colloid Interface Sci. 142, 369 (1991).
19. M. Yasrebi, W.Y. Shih, and I.A. Aksay, J. Colloid Interface Sci. 142, 357 (1991).
20. W.L. Vaughn and H.G. Maahs, J. Am. Ceram. Soc. 73, 1540 (1990).
21. R.M. Horton, J. Am. Ceram. Soc. 52, 121 (1969).
22. M. Mitomo and J.H. Sharp, Yogyo-Kyokai-Shi 84, 33 (1976).
23. T. Sato and K. Fujii, Yogyo-Kyokai-Shi 90, 110 (1982).
24. H. Du, R.E. Tressler, K.E. Spear and C.G. Pantano, J. Electrochem. Soc. 136, 1527 (1989).
25. W. Jander, Z. Anorg. Allgem. Chem. 163, 1 (1927).
26. E.W. Sucov, J. Am. Ceram. Soc. 46, 14 (1963).
27. F.J. Norton, Nature 191, 4789 (1961).
28. S. Wu and N. Claussen, J. Am. Ceram. Soc. 74, 2460 (1991).
29. I.A. Aksay, in *Ceramic Powder Science II*, Ceramic Transactions Volume 1, G.L. Messing, E.R. Fuller, Jr., and H. Hausner, Eds. (The American Ceramic Society, Ohio, 1988) pp.663-674.